Fatigue Considerations of High Strength Rolling Bearing Steels

Gabriel F. Dambaugh, P.E.

gabe@feaservices.net
www.feaservices.net

.

Abstract: Since the 1946 issuance of the ASTM bearing steel specification, A295, the research and development of bearing steels has resulted in substantially improved fatigue and wear performance of rolling bearings across the entire industry. This is not only the case with higher-end "advanced" materials and processes such as ceramic based technologies, but also with the more economic material selection of bearing quality steels.

The bearing quality steels are characterized primarily, though not exclusively, by high hardness, very high static strength, fine grained microstructures, and low non-metallic inclusion content. Although developed to perform under cyclic rolling contact and slippage loads, these steels are also at times considered for usage in structural applications, such as shafting. When used in a structural manner, the design engineers are advised to consider unique fatigue related attributes of rolling bearing steels, such as the concept of "volume stressed".

The main point presented is that bearing grade steels in structural applications are expected to realize a wide range of cycles to failure in a group of seemingly identical parts. Also discussed are some related experiences with Virtual Product Development activities at INA (Schaeffler) USA with bearing/structural components using a combination of FE analysis with ABAQUS, fatigue assessment and validation testing.

1. ROLLING BEARING STEEL FATIGUE BASICS

1.1 INTRODUCTION

In making fatigue endurance considerations with high strength rolling bearing steels for use as a potential material for structural applications, it is worth examining the wealth of experience found from the theory and practice of using these steels in their native application. Thus, a short background regarding the mechanics of bearing fatigue, the materials used, and some common key effects on the fatigue life of rolling bearings is provided.

For the purpose of this paper, a "structural" type loading application is defined as one where a mechanical member, such as a shaft, supports cyclic bending and/or shear loads. This is important to note since we are drawing connections to the fatigue life of rolling bearings, which see mainly only compressive load cycles, to the fatigue life of those same steels when used under tensile and shearing conditions. For the balance of the paper, "bearing" and "bearing steels" will be used interchangeably with "rolling bearing" and "rolling bearing steels", respectively.

It is assumed for this paper that the reader has some knowledge of the assembly and basic function of a rolling bearing. An important consideration of the fatigue process is that the bearing loads are transmitted through one or more of the *rolling elements*, and the two adjacent *races*. The purpose of a rolling bearing is to eliminate friction between machine components that move or rotate in relative motion under load. For an introduction or a study of bearing design and analysis, the reader may consult Harris (1991) or Eschmann (1985).

1.2 A PRIMER ON BASIC ROLLING BEARING FATIGUE MECHANICS

A starting point in understanding the mechanics of bearing fatigue is the concept of sub-surface stress due to contact of curved surfaces. Although several potential "failure" mechanisms such as denting, false brinnelling, or a host of others (Tallian, 1999) can occur in a bearing application, classical material fatigue cracking typically develops at *or beneath* the surface of the load-bearing rolling elements and their contacting raceways as shown in Figure 1.

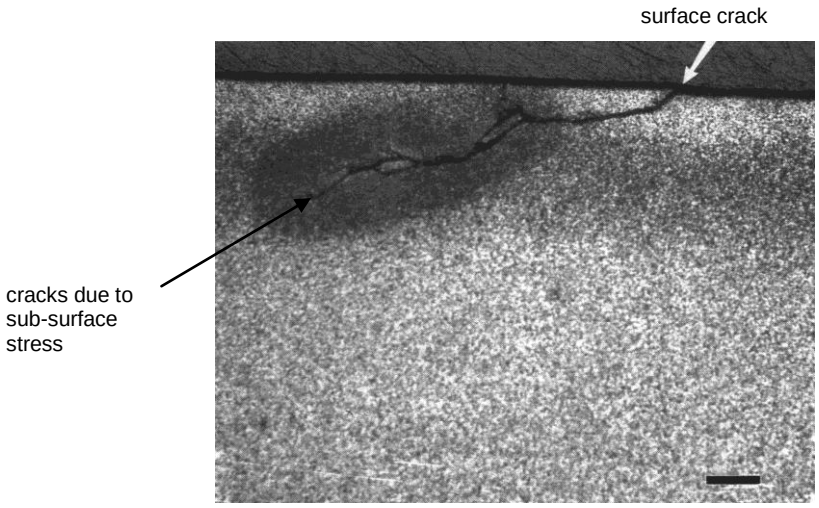

Figure 1. Sub-surface fatigue cracking. Etched, note tempered martensite microstructure. Reprinted (Tallian, 1999) with permission granted by ASME Press.

Contact pressure, which is defined as the normal stress into the surface at the point of contact, is developed between the curved surfaces according to the theories of Hertz (1896). Stress tensors in the volume beneath the surfaces in contact are derived from the pressure, area developed, and material in contact (Jones, 1946).

Some of the basic analytic equations for contact involving cylindrical roller, needle roller, and ball bearings as extended from *Hertzian* theory (Hertz, 1896 and Jones, 1946) provide a means of basic mechanical analysis. The derivation and assumptions used to arrive at the basic equations long used for analysis by bearing engineers are provided by Harris (1991). Considering for now a "point" loaded contact between two solid spheres, (Figure 2) the resulting basic equations (Shigley, 1989) of interest include:

- Width of contact area:

$$a = \sqrt[3]{\frac{3F}{8}\frac{\left(1-\nu_1^2\right)E_1 + \left(1-\nu_2^2\right)E_2}{1/d_1 + 1/d_2}} \tag{1}$$

- Maximum contact pressure:

$$p_0 = \frac{3F}{2\pi a^2} \tag{2}$$

- Coordinate stresses on the normal axis: (Figure 3)

$$\sigma_x = \sigma_y = -p_0\left[\left(1 - \frac{z}{a}\tan^{-1}\frac{1}{\left(\frac{z}{a}\right)}\right)(1+\nu) - \frac{1}{2\left(1+\frac{z}{a}\right)}\right] \tag{3}$$

$$\sigma_z = \frac{-p_0}{1+\frac{z^2}{a^2}} \tag{4}$$

where: F = applied load, ν = Poisson's ratio, E = elastic modulus, d = diameter, z = depth into surface.

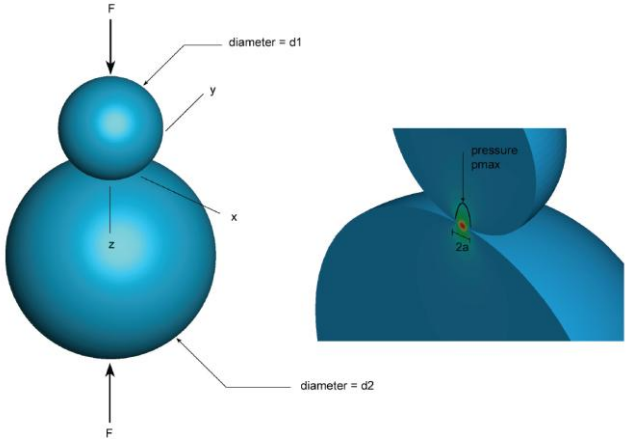

Figure 2. Contact area (2a) developed between spherical surfaces with diameters d1 and d2, under load. FEM view on right shows pressure at small contact area.

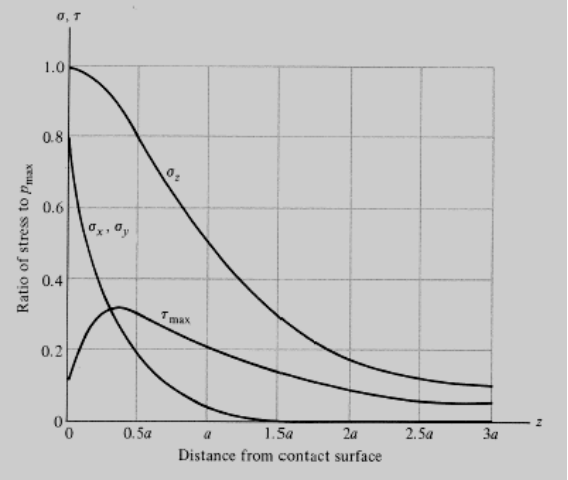

Figure 3. Sub-surface coordinate and shear stress relationship for loaded spheres. (e.g. ball bearing) Note that p_{max}, σ_z σ_x and σ_y are all in compression.

The coordinate stresses, which are all compressive, define the stress state at any point beneath the surface of contact along the axis of applied load, F. Figure 3 shows a plot of these coordinate stresses as well as the calculated maximum shear stress, $\tau_{\max}$, as a function of the distance beneath the surface. It is seen in Figure 3 that the maximum value of $\tau_{\max}$ lies beneath the surface. Although not shown above, the maximum distortion energy (also known as Von-Mises) stress is also located beneath the surface, at a depth very close to the depth of maximum shear.

Here lies the importance of the concept of sub-surface stress in the study of bearing mechanics: It has been generally found in the study of ductile metal failure (such as steel) that *deviatoric* components of the stress tensor are responsible for the onset of metal plasticity, not by the *hydrostatic* stress components (Shigley, 1989 and Stephens, 2001). It has also been widely adopted in structural metal fatigue concepts that fatigue is generated in an area of a mechanical member that sees plasticity, or the development of *slip-bands* under cyclic loading, typically occurring in small areas of a structure such as a "stress riser" or other discontinuity (Dieter 1986, and ASM 2002). With this connection to structural fatigue in mind, it becomes easier to understand why the origin of classic bearing fatigue begins beneath the surface; this is where the shear and Von-Mises stresses are the greatest.

Pre-modern bearing fatigue theory, whose roots still pervade the more modern theories and ISO standards, (ISO 281, 1990) considers the maximum *alternating* shear stress as the critical influence on sub-surface bearing fatigue (Lundberg, 1947). The shear stress parallel to the surface, τ_{zy}, actually reaches a maximum, $\tau_{zy-\max}$, at a point near the edge of the contact area per Figure 4 and directionally cycles as the rolling element passes through the loaded contact zone. The calculated depth of this critical point is slightly closer to the surface (0.50a vs. 0.78a) than with the maximum shear ($\tau_{45-\max}$) theory.

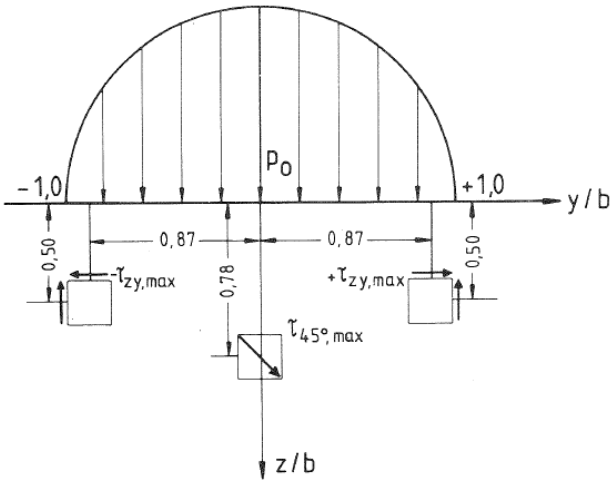

Figure 4. Sub-surface shear stresses assuming zero traction forces at surface. Reprinted, with permission, from STP 987 Effect of Steel Manufacturing Processes on the Quality of Bearing Steels, copyright ASTM International, 100 Barr Harbor Drive, West Conshohocken, PA 19428.

Of key importance to this background is that from the late 1940's work of Lundberg and Palmgren, (1947) we get the connection of the fundamental law of Weibull theory, (Weibull, 1939) which describes the *probability* of rupture due to a *distribution* of stress over a *volume*, to a useful bearing fatigue life theory. The Weibull function so noted is:

$$\ln\left(-F^*\right) = -\int_V n\left(\sigma\right) dv \tag{5.1}$$

Lundberg expanded Weibull's function to describe the condition of the material over N cycles of loading and combined the theory of alternating shear stress damage through a sub-surface depth of z_0 into the equations to arrive at the function:

$$\ln\frac{1}{S} = f\left(\tau_0, N, z_0\right) \tag{5.2}$$

With empirical data, Lundberg et al. (1947) found a relationship to fit their real bearing test results and arrive at a most important relationship between the probability of rolling bearing fatigue failure, to the applied stress and *volume stressed*. This relationship can be written as follows:

$$\ln\frac{1}{S} \sim \frac{\tau_0^c \cdot N^e}{z_0^h} \cdot V \tag{5.3}$$

where:

$F^* = \text{probability of failure}, V = \text{volume affected}, S = \text{probability of survival},$
$\tau_0 = \text{maximum alternating shear stress } (\tau_{zy} \text{ in Figure 4}),$
$h, c = \text{empirical constants},$
$e = \text{Weibull distribution (slope) of rolling bearing fatigue life}.$

The main point to be taken from relationship 5.3 for is that the probability of fatigue survival (of the bearing) is inversely related to the volume stressed. As the affected sub-surface stressed volume increases, the probability of survival decreases.

Further derivation from relation 5.3 is provided by Harris (1991) to the simple universally used rolling contact bearing fatigue life equation, in which the effect of volume stressed is linked via the bearing *capacity*. Written in the more common industry standard form, this equation is:

$$L = \left(\frac{C}{P} \right)^p \tag{6}$$

where:

$L = \text{fatigue life of bearing, in millions of cycles, at 90\% reliability } (L_{10}),$
$C = \text{bearing capacity, depending upon bearing size and geometry (ISO 281, 1990)},$
$P = \text{applied load to bearing},$
$p = \text{exponent per bearing type (3 for ball bearings, 10/3 for roller bearings)}.$

1.3 SCATTER IN ROLLING BEARING FATIGUE RESULTS

Weibull reliability analysis (Harris, 1991, Eschmann 1985, Murthy 2003, Weibull, 1951) is well known in the fatigue testing world, and is a primary means of evaluating bearing fatigue results. Weibull analysis of fatigue testing provides a wide range of reliability assessments as well as being an economic testing method. In rolling bearings, the reliability is vital to the discussion of how much service life can be expected from a bearing design due to a wide range (scatter) of fatigue results found from experience.

Figure 5 from Eschmann (1985) shows a scatter plot from a test of thirty (30) 6309 ball bearings run until fatigue failure. These parts are said to be nearly identical, and were run under identical conditions. From this data, it is seen that the shortest run time was about 15.e6 cycles while the longest run time was 300.e6 cycles, a 20:1 range. This scatter is considered typical from bearing experience; other similar examples are provided by Harris (1991). Due to the wide scatter, it is clear that predicting a service life for a single bearing is not possible, and that statements on fatigue life can only be made in terms of expected *reliability*.

The explanation for the wide scatter is that few "weak" points exist in the design geometry, the manufactured surfaces, and in the base material. With few weak points present in the components

from which stress risers (however small) could develop to initiate fatigue, then an "early" fatigue crack will develop very seldom, and in a random fashion such as (perhaps) the part that ran only 15.e6 cycles per Figure 5. Longer running parts likely have their own weak points in areas of lower stress; fatigue is still developed in these regions, but over more cycles. How the condition of the base material can affect the observed scatter range will be discussed in later sections of this paper. It should be noted, however that this wide scatter is one of the main considerations when using high strength bearing grade steels in structural fatigue applications.

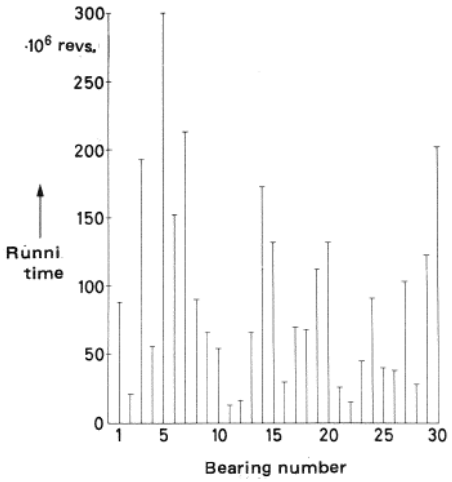

Figure 5. Scatter plot of 6309 bearing fatigue results under identical test conditions. From Eschmann (1985) Copyright John Wiley & Sons, Ltd. Reproduced with permission.

As noted above, a widely used tool for bearing reliability is Weibull analysis. In the basic Weibull form, data points (fatigue failures) are plotted on a log scale for the run time on the abscissa, with the ordinate representing the failure probability as log ln[1/(1 – F(t))] for the failure probability:

$$F(t) = 1 - \exp[-(t/T)^k] \tag{7}$$

where T is the point which 63.2% of the samples have failed and k corresponds to the gradient of the plotted straight line. A large k indicates less scatter while smaller k values indicate more scatter. For rolling bearings, k is slightly above 1 (1.11 – 1.35) depending on the bearing type (Eschmann, 1985). Each running time, t, is plotted accordingly to develop the final Weibull plot as shown in Figure 6.

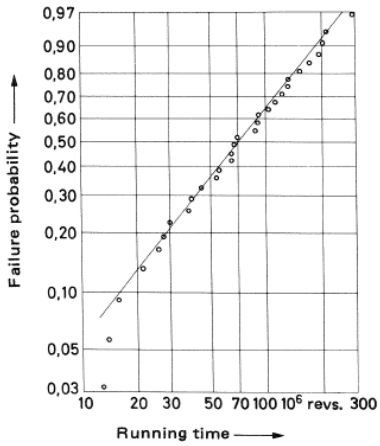

Figure 6. 6309 test results charted with Weibull parameters. From Eschmann (1985) Copyright John Wiley & Sons, Ltd. Reproduced with permission.

As a side note, instead of evaluating scatter on the basis of the Weibull slope, one can also compare the L_{50} (median life) to the L_{10} (90% reliable) results of a fatigue test. For rolling bearings, the standard *expected* L_{50} is 5 times greater than L_{10}, or a 5:1 ratio (Harris, 1991). The 6309 parts noted above had a L_{50} to L_{10} ratio of 70e6/17e6 = 4.1:1.

The experiences of very wide bearing fatigue scatter, greatly due to the nature of the material, is something to be considered when using the same material in a machine component *structural* type application. The nature of these bearing quality steels is discussed in the following section.

1.4 DISCUSSION OF ROLLING BEARING STEELS

The basis of the high load carrying capability and reliable function of rolling bearings is the steel from which they are produced. From a mechanical viewpoint, bearing grade steels are mainly characterized by high hardness (HRC58-65) and very high tensile strength. Excellent wear properties and rolling contact fatigue endurance with reasonable impact resistance can also be expected. It is the final manufactured *microstructure* of the steel that ultimately provides the necessary mechanical properties desired, or rather required. Note that for the remainder of this paper, we will mainly consider high-carbon through-hardening alloyed steel, SAE52100 and its equivalents, as it is still the most widely used bearing grade steel across the industry (Harris 1991, Voscamp, 1988, Pearson 1988).

Now considering the microstructure from the metallurgic point of view, bearing grade steel microstructures in an optimal condition are characterized by (Voscamp, 1988, Pearson, 1988, Carpenter, 2006, ASTM A295-98 and A485-94) :

- BCT tempered martensite microstructure (Figure 7)
- Fine grain size: ASTM 8 or finer (ASTM E112-96)
- Fine and uniform distribution of carbides

- High degree of "cleanliness", i.e. tightly controlled non-metallic inclusion content

With a fine grain size, it is expected that the 52100 should exhibit high static strength. It has long been understood that finer grains in ferrous metals produce higher static and fatigue strengths (Dieter 1986, Hertzberg, 1996, Socie, 2000). It must also be emphasized that the high strength of martensite is due to several mechanisms (Hertzberg, 1996) and that for the purpose of this paper we will mainly consider the end results. With tensile strength (S_{UT}) for example, it has been found that strengths of up to 2550 MPa (370 ksi) can be realized for 52100 with the proper combination of austenitizing and tempering temperatures (Zwirlein, 1976 and Stangner, 1986). INA USA testing has verified these strengths using similar heat treatment combinations. This high strength is indeed indicative of relatively long expected running times of a rolling bearing.

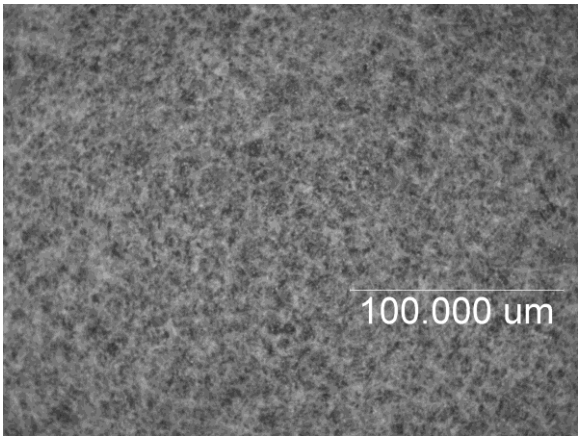

Figure 7. Micrograph of a typical tempered martensite microstructure showing fine and uniform carbides. Photo by INA USA.

In the previous section, data pertaining to bearing life scatter was discussed. The main reason for the bearing fatigue scatter lies in the microstructure, or rather, random *inhomogeneities* in the microstructure. Some forms of inhomogeneities include pores and banding (Harris, 1991) both of which are caused by improper solidification processes, and thus can be controlled during steel processing. The more common known sources of an in-homogenous local volume in the microstructure are non-metallic inclusions. The content of these inclusions are tightly controlled in bearing grade steels (ASTM A295-98 and A485-94) yet they still exist with present technology, however small in number and size.

Since the middle of the 20th century, bearing steel producers have taken steps to improve methods for reducing the content of non-metallic inclusions, with the result being greater and more reliable bearing durability across the entire industry (Green, 1998). For example, during the 1960's it became increasingly popular to utilize vacuum degassing and vacuum melting systems, such as VIM and VIM-VAR processes to produce bearing quality steels with a high degree of cleanliness (Harris 1991, Green 1998, Zaretsky 1988). Research on how these processes affect the quality of bearing steels ensued, which resulted in many documented cases of correlation between bearing fatigue lifetime and inclusion content. It is now generally understood from these efforts that the

purity of the steels has a significant effect on fatigue life and scatter. Some of this research is presented in the selected references (Schlicht, 1988, Hampshire, 1988, Monnot, 1988, Zaretsky, 1988, Lormand, 1998) and will be discussed further in the next section.

1.5 INCLUSION EFFECT ON BEARING LIFE

As the elastic continuum beneath the surface of a bearing race is stressed by the contact pressure in a rolling bearing application (Figure 4) any discontinuity in the otherwise homogenous structure will result in even higher stresses, or a *stress riser* around that discontinuity. Local plastic deformation is another likely result around such a stress riser. A non-metallic inclusion in an otherwise highly clean microstructure is one such discontinuity that *naturally exists* in bearing steels, even after the manufacturing efforts mentioned in the previous section are made to eliminate them. The research previously referenced strongly supports the common knowledge that classic bearing fatigue often originates at an inclusion. This was actually understood by the first half of the 20th century, prompting issuance of the ASTM specification A295 in 1946 (Green, 1998).

Figure 8 shows a section view through a fatigue "spall" of a bearing race, where the crack origination is sub-surface at a point corresponding to a trail of alumina type inclusions. From experience, the shape and nature of the pitting seen at the race surface is typical of classic bearing fatigue per this photo.

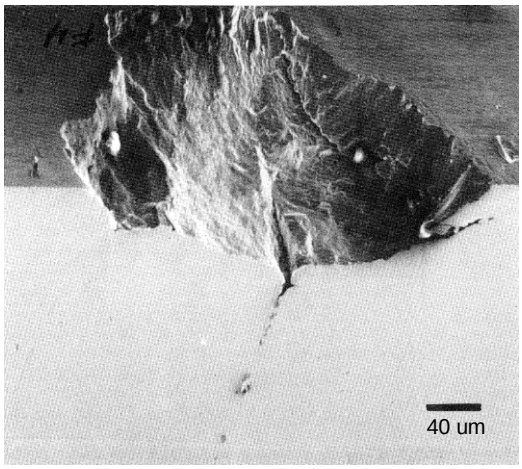

Figure 8. Section through bearing fatigue spall showing inclusion trail in area of high shear stress. Reprinted, with permission, from STP 987 Effect of Steel Manufacturing Processes on the Quality of Bearing Steels, copyright ASTM International, 100 Barr Harbor Drive, West Conshohocken, PA 19428.

Reviewing Figure 8 and holding the "stress riser" concept in mind, it is logical for an engineer in any industry to deduce that with a reduction of such non-metallic inclusions, longer bearing life is expected. The research indeed supports this; test data from one such study of inclusion content

effect on life is provided in Figure 9 (Schlicht, 1988) where a lower summation of "cleanliness" essentially denotes fewer inclusions.

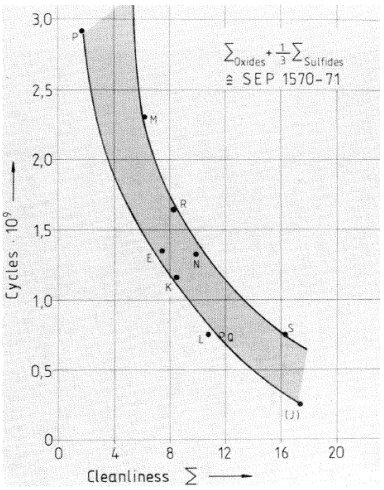

Figure 9. Test results showing reduced bearing fatigue lives with increased inclusion amounts. Reprinted, with permission, from STP 987 Effect of Steel Manufacturing Processes on the Quality of Bearing Steels, copyright ASTM International, 100 Barr Harbor Drive, West Conshohocken, PA 19428.

We now come to an explanation of wide bearing fatigue scatter taken from the data presented above: Since modern bearing steels are produced with relatively tight yet imperfect controls on allowable inclusion levels and sizes, (ASTM A295-98 and A485-94) a "critical" inclusion will exist in a "critically stressed volume" on *a random basis only*. When such a discontinuity does *not* exist in the critically stressed volumes, again due to the high degree of steel cleanliness, we often get significantly longer running times compared to the L_{10} of the bearing group. For example, if we compare *calculated* L_{90} versus *calculated* L_{10} per Harris (1991), that ratio is approximately 14:1.

At this point it must be duly noted that geometry and surface variation can also cause *some* bearing scatter. However, the surface condition of most modern rolling elements and races in a typical industry standard bearing is of very high quality such that it is not expected that surface finish variation will result in a large percentage of the scatter typically experienced. Similarly with geometric variation, some scatter is expected, but very fine tolerances are controlled within a given manufactured lot. For example, INA produces needle roller bearings with *no more than* a 2µm total variation in roller diameter in any given bearing as a base standard. Finally, variances in lubrication conditions, test rig setup, etc. from part to part within a given group, also play some role regarding bearing fatigue test scatter.

One of the main points presented here is that *intrinsic to the base metal and processing of the material itself*, lies a feature (non-metallic inclusions) which will often result in relatively wide scatter in fatigue results in bearing applications. One is advised to consider this scatter, and its

reasons, when using high strength bearing quality steels in other types of structural machine component applications.

2. BRIDGING THE EXPERIENCE OF ROLLING BEARING FATIGUE TO STRUCTURAL FATIGUE WITH HIGH STRENGTH BEARING STEELS

2.1 FATIGUE CONSIDERATIONS OF STRUCTURAL MACHINE APPLICATIONS

We shift our attention now to more general structural fatigue type applications while drawing from some of the bearing related points as discussed in Part I. That is, what lessons from bearing technology related to fatigue are most advised to take into consideration when using high strength bearing quality steels as structural machine members? To provide some bridges in that regard, experiences from the bearing industry are now shared to help make appropriate comparisons and connections.

2.2 COMPARISON TO STRUCTURAL FATIGUE: SUB-SURFACE VS SURFACE

As discussed previously, it is well established that inclusions existing in the base material play a vital role in the fatigue life of a rolling bearing, and that these failure points usually initiate *beneath the free surface*. Here then is one distinction between structural and bearing fatigue: In the field of structural fatigue, it has long been accepted that fatigue cracks almost always initiate *on the free surface* (Dieter, 1986, Socie, 2000, Forrest, 1962). This distinction can be explained by review of some facts from the basics: With bearing loads, the highest critical stress is *beneath* the surface, while with most other structural applications, the highest critical stress is *at* the surface. Furthermore, crack initiation at the surface of a structural application is accelerated by *surface finish effects* (Shigley, 1989, Dieter, 1986, Juvinall, 1991) unless the surface is conditioned so well as to have a so-called "mirror polish" with zero imperfections whatsoever for a fatigue crack to nucleate from.

Thus, the next point to consider when using high strength rolling bearing steels for structural applications is that a fatigue crack can originate at or *beneath* the surface when cyclically loaded, for example in bending. The potential influence of sub-surface inclusions must still be considered when using bearing grade steel for a structural member. This is in contrast to more ductile steels since it has been found that fatigue endurance of "soft" steel is "little affected" by inclusions (Forrest, 1962).

From a discussion on data scatter related to structural applications, Juvinall (1991) states that "…fatigue failures originate at *local* points of relative weakness…" Given the very high strength of the base microstructure, and assuming that a finely ground or better surface is produced, the fatigue failure mode of bearing steels in a structural application can still be from sub-surface inclusions as opposed to surface nucleates. At these stress risers, it is likely that local plasticity develops around the edges of the inclusion, corresponding to an accepted phenomenon that structural metal fatigue often originates from areas of localized high strains, often plastic in nature (Stephens, 2001, Socie, 2000, Juvinall, 1991). Supporting evidence from bending fatigue tests of bearing grade SAE52100 steel made at INA USA is presented here. In these tests it was found that the bearing grade 52100 steel exhibited very high fatigue strength yet was susceptible to

random fatigue failure from critical inclusions existing in the stressed volume. It was discovered that the fatigue failures did not originate from surface nucleation points, but rather from sub-surface stress risers due to non-metallic inclusions just over 10 microns in size.

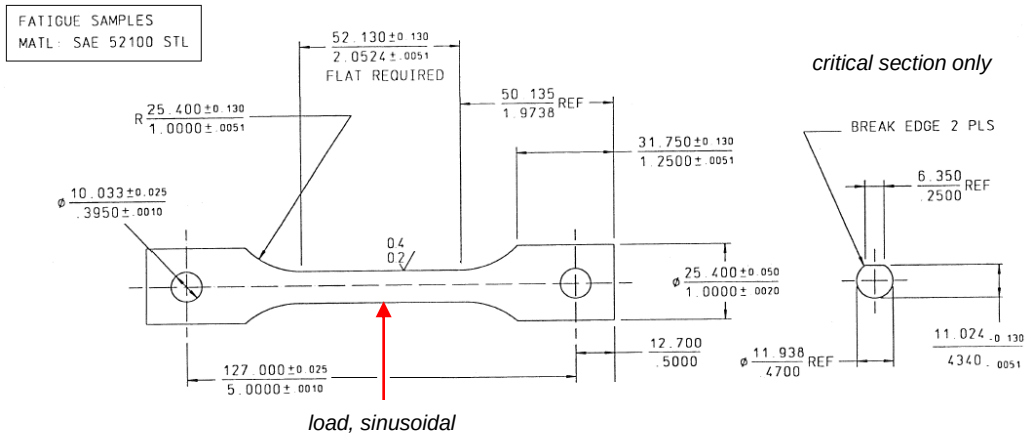

Figure 10. INA USA SAE52100 test sample sketch.

For these bending tests, samples from a single heat of 52100 were machined to the configuration as shown in the sketch per Figure 10 and heat treated to a hardness range HRC60-64. The sketch shows a flat on the critical surface opposite of the applied load, which is centered between the supporting 10mm pins, spaced 127mm apart. The purpose of the flat section was to increase the amount of volume stressed in the critical area. The samples were loaded in bending, with a hydraulically actuated MTS machine, such that a theoretical sinusoidal pulsating tensile stress from 0 to 221.5 ksi (R=0) was applied to the flat area in the center of the test beam. The flat itself was finely ground with the surface being controlled such that the resulting R_a values were on the order of 0.2 microns.

By utilizing standard textbook fatigue assessment procedures, for example a typical modified Goodman method (Shigley, 1989) the expected fatigue approximation would suggest that these samples would not be expected to reach 1e6 cycles before failure as a median (L_{50}) result. However, the real parts performed better than "expected" with L_{50} fatigue results >1e6 cycles as seen by the Weibull plot of the test results as provided in Figure 11.

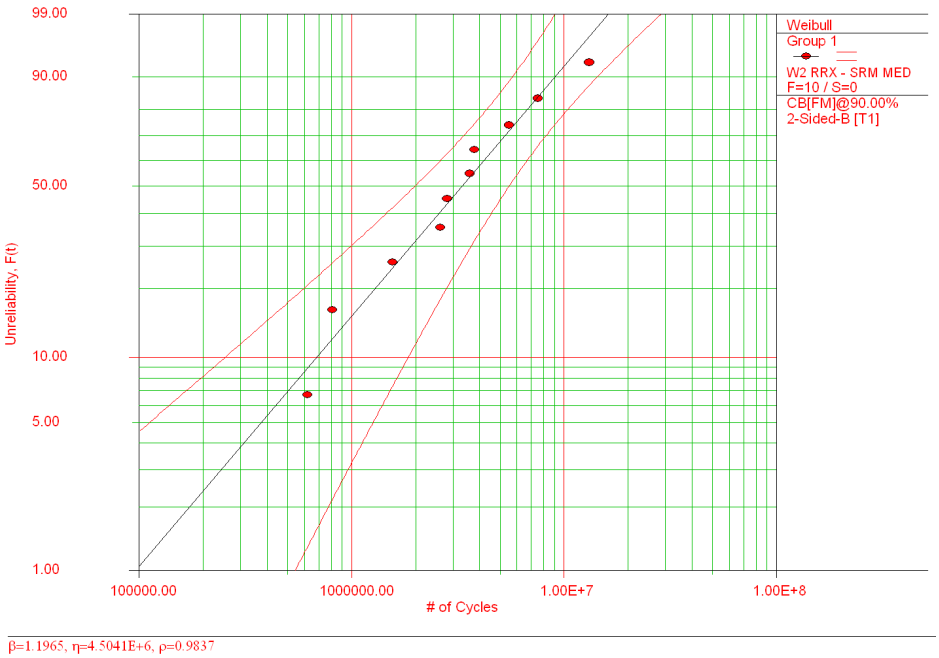

Figure 11. INA USA SAE52100 bending test fatigue results from 1997-1998. HRC60-64, σ_{max} = 221,500 psi, R = 0. Note slope, β=1.196.

Only two of the ten tested samples failed under 1.e6 cycles and the L_{50} result (Figure 11) was over 3.e6 cycles. A key point is that the testing resulted in a Weibull slope of just over 1, (1.196) which is what is experienced in rolling bearing tests. Also note the range from high to low was 21:1 over 10 pieces, (13.1/0.62) again similar to bearing test experience and calculations, as discussed in Part I. The common thread in this comparison is the nature of the material.

The location of the fatigue origination points in the bending tests presented is also of key interest. With the "calculated" fatigue safety factor being less than 1, we would typically expect fatigue cracking to originate *at the free surface* in a structural bending application (Dieter, 1989 and Socie, 2000). However, as noted previously, bearing grade steels are susceptible to fatigue failure due to intermittent sub-surface inclusion content, even though this content is kept to a minimum by the industry. For the INA USA SAE52100 bending tests as presented here, all of the samples were found to fail at origination points clearly beneath the surface of maximum stress, all at a non-metallic inclusion as shown in Figure 12. Hence, when using bearing grade steel in structural applications, one must expect the potential for a high scatter of fatigue cycles to failure, in large part due to the variance of steel cleanliness in the critically stressed volume from part to part.

Figure 12 shows SEM photographs taken from the fracture surface which reveals a TiCN (titanium carbo-nitride) inclusion on the order of 10 microns long at the center of the fatigue origination point.

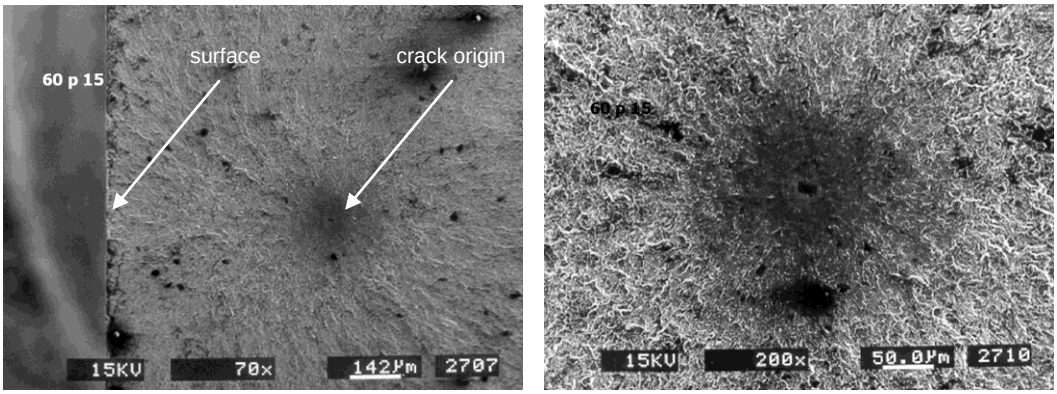

Figure 12. From INA USA testing, SEM photos (70x left, 200x right) showing sub-surface origination of fatigue failure at non-metallic inclusion of 52100 sample.

Upon further inspection of the fracture surfaces per the SEM photos, it is believed that the likely sequence of events was as follows:

1. The original crack developed at the edges of the TiCN inclusion, followed by

2. Crack progression over more cycles until a critical internal crack size is reached

3. Finally, the size of this internal crack reaches a critical length (about 100 – 200 microns) resulting in sudden fracture of the entire section around the seemingly small crack.

The reader may consult the references (Dieter, 1986, Hertzberg, 1996, Stephens 2001) in the study of fracture mechanics to review how greatly a crack of the size and shape as seen in the SEM photos above can adversely affect materials of very high strength, i.e. those with low K_c values, such as bearing grade SAE52100.

In summary, the experience gained from the structural testing presented here helps to support the main fatigue related connections between rolling bearing and structural applications with bearing grade steel:

- As with bearing applications, bearing grade steel provides excellent fatigue durability properties under "structural" fatigue loading conditions.
- As with bearing applications, a high range of fatigue scatter, with Weibull slopes on the order of 1, is to be expected in "structural" applications.
- Fatigue crack origination can develop sub-surface at inhomogeneities in the microstructure, such as non-metallic inclusions. This phenomenon is seen in bearing applications as well as in structural fatigue testing and contrasts to the understanding of the effect of similar inclusions in more ductile steels.

2.3 HARDNESS EFFECT ON STRUCTURAL FATIGUE RESULTS

It is well accepted that a geometric discontinuity, more commonly called a "design notch", such as a fillet or hole, creates a stress riser by *design* when located in the load path of a structural member. Stress risers also arise from surface imperfections and sub-surface discontinuities. Thus, in a qualitative sense, the effect of surface roughness and/or sub-surface inclusions can be thought to have similar relative effects on the fatigue strength of a part as design notches (Dieter, 1986); in either case it is understood that a local plastic zone develops in a small area where fatigue is initiated over many load cycles.

The *reduction in the material fatigue endurance* behavior, or *sensitivity* to notches, has been well documented to be a function of the material tensile strength or hardness. As presented in the data from Figure 13, notch sensitivity has been found to increase with tensile strength and hardness (Shigley, 1989, Dieter, 1986, Stephens, 2001, Juvinall, 1991). Basically, machine elements with higher strength/hardness will realize a more drastic reduction in fatigue endurance due to the presence of notches (or similar stress risers) as compared to a more ductile material.

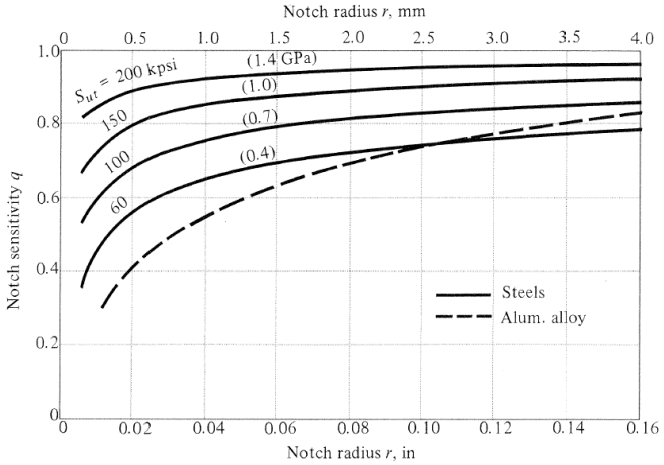

Figure 13. Notch sensitivity (q) as a function of notch radius and strength. Higher sensitivity relates to greater *reduction* of fatigue strength.

A physical understanding of this phenomenon might be learned from the concept of "crack tip blunting" of ductile metals (Dieter, 1986, Laird 1979, Laird, 1967) and cyclic plastic zone size (Stephens, 2001). In short, the crack tip in a stronger (more brittle, less ductile) steel would have a smaller plastic zone thus *tend not* to undergo a plastic blunting process such that once a fatigue crack is formed, it will extend into the critical cross section from less applied energy than a ductile steel. Dieter (1986) even states on the topic "…Thus it is possible in certain circumstances to *decrease fatigue performance* by *increasing the hardness* or tensile strength of the material…"

Another main point of consideration when using bearing grade steels as a cyclically loaded structural member in a machine component is that due to the effect of notch sensitivity is:

- In comparison to more ductile steels, the very high hardness and strength of bearing grade steels make it imperative to consider the potential damaging effects of imperfect surfaces, design notches, or inclusions, on fatigue endurance and scatter.

The purpose of this section is not to prove how the hardness of the steel relates to fatigue results, but rather to present test data concerning bearing grade steel loaded in a structural manner. INA USA conducted some fatigue testing to investigate notch effect vs. hardness of a typical bearing grade steel and to support the above mentioned point of consideration. The test data presented below is from a low carbon carburizing grade bearing steel used for drawn cup bearings.

Flat test coupons (samples) were stamped from strip stock and notched in the center per the sketch shown in Figure 14. All samples were made from the same low carbon steel coil in the manufacturing run. The samples were sorted into two groups, the difference between the two being heat treatment only. One group was heat treated (carburize, quench, and temper) to a final surface hardness in the range of HRC60-64; the exact hardness is not published here. Group 2 was heat treated to a surface hardness of HRC48. The case depth was sufficiently deep to prevent failure initiation from the softer "core" material. The samples were then cyclically loaded with a hydraulically actuated MTS machine, under pulsation with R=0.15, such that the small notched radius was located at the point of maximum tensile stress from the bending load.

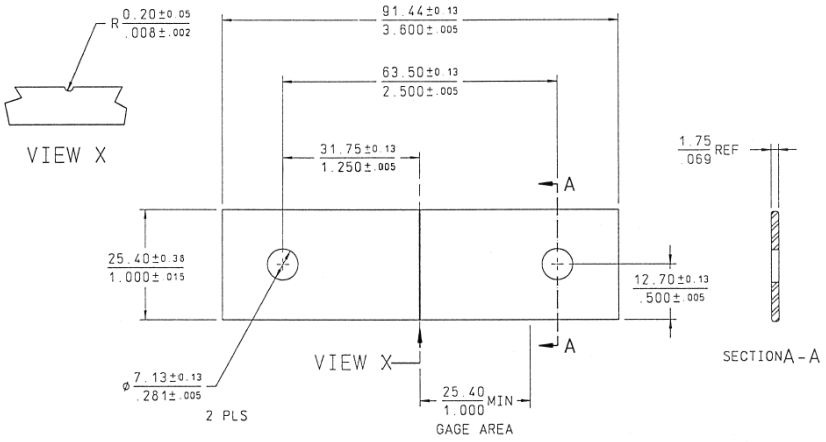

Figure 14. INA USA Low carbon steel notched test coupon sketch.

The results from the bending fatigue tests of the carburized steel samples are provided in the Weibull plot per Figure 15. The Weibull slopes are 7.25 and 1.76 for the HRC48 and HRC60-64 samples, respectively. This data supports the idea that with more ductile steels, as opposed to higher hardness steels, fatigue data will tend to exhibit significantly less scatter since the ductile material is *less sensitive to notches*, and therefore less affected by the *randomness* of discontinuities during the first stage of fatigue: *crack initiation*.

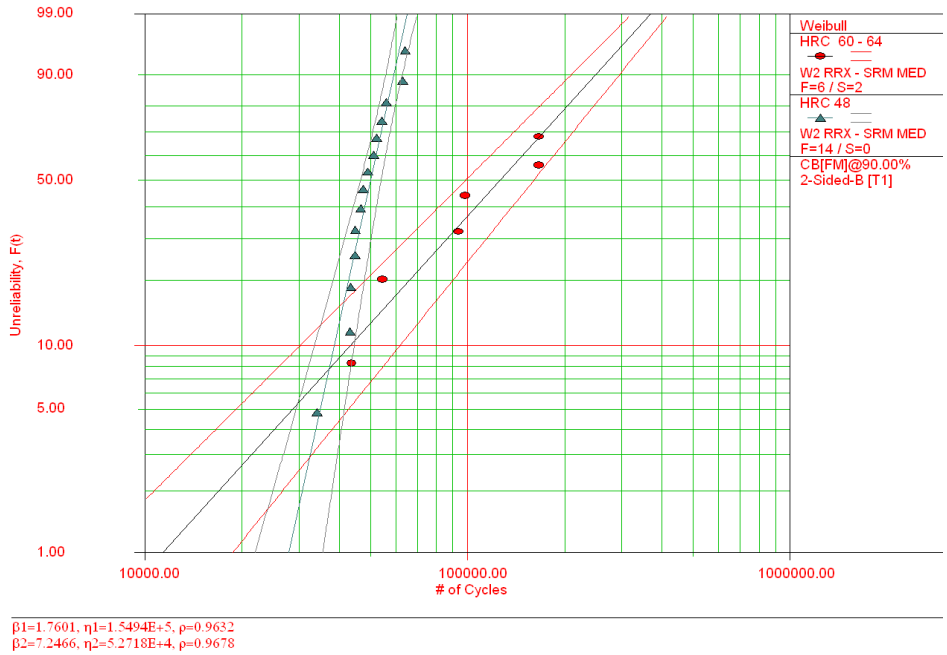

Figure 15. INA USA Carburized steel bending fatigue test results. HRC60-64 samples compared to HRC48, R = 0.15, Note slope difference, β2> β1.

Other interesting points taken from the test data are as follows:

1. Upon inspection of the fracture surfaces of the tested samples, surface initiated fatigue is suspected although the cross sectional geometry makes these inspections less than certain. No core initiated failures were observed.
2. Resulting L_{10} between the two hardness groups are nearly the same, around 40K cycles.
3. Median lives (L_{50}) between the two groups differ by nearly 2.5:1. (120K for HRC60-64 samples vs. 50K for HRC48 samples)
4. Two (2) samples from the HRC60-64 group were suspended at 2.e6 cycles, showing a very high range (45+:1) of individual fatigue cycle results with "high" surface hardness. This compares to a range of approximately 2:1 (14 samples) from the HRC48 parts.

In summary, the higher hardness (higher tensile strength) bearing grade HRC60-64 test samples did in fact show a median fatigue life improvement compared to the softer HRC48 samples. However, higher scatter can make the assurance of high reliability more difficult to assess from limited sample testing. Note that because it is difficult at best to get the surface residual stress accurately within the small notch (Figure 14) we are unable to report any potential residual stress difference between the two groups at the area of interest.

Even without *design* notches, it still makes sense that ductile steel will exhibit less fatigue cycle randomness compared to higher hardness (more brittle) steel for cycles to final fracture. This is

due in part to the fact that during stage 2 of fatigue, *crack propagation*, a fatigue crack in more ductile material will require more load cycles to extend to the "critical" length required for final fracture. One way to understand this is through the concepts of fracture mechanics as mentioned previously. Since ductile steel has significantly higher K_c values as compared to bearing grade steel, the critical crack length for fracture is larger for ductile steel. The total fatigue cycles until final fracture (stage 3) for ductile steel is therefore *relatively dominated* by stage 2 cycles, as compared to "brittle" (high hardness) steel. This tends to reduce the effect of "stage 1 randomness" on the *total* cycle randomness to final fracture for ductile steel.

Conversely, the total fatigue cycles of more "brittle" steels are *relatively dominated* by stage 1 initiation, thus more total randomness is expected since it is at or near the surface where variations due to manufacturing processes exist, in turn randomizing fatigue nucleation occurrences.

2.4 STRUCTURAL MACHINE APPLICATIONS WITH BEARING GRADE STEEL

Because of the inherent scatter and fatigue sensitivities regarding very high strength steels as discussed thus far, it may seem clear to the reader that the use of bearing grade steel does not appear to be a good choice compared to traditional "tough" structural steels when high reliability in a structural machine application is required. In some applications, however the use of bearing grade steel is either inevitable, or the best economic solution. Some machine element examples from situations where bearing steel serves as a structurally loaded member are listed here:

1. Shafting: Radial bearings often run directly on a shaft surface as the bearing raceway while the shaft also simultaneously supports cyclic bending loads.

2. Cylindrical Roller Bearing Flanges: Certain radial bearings must support cyclic thrust loads against a flange, such as cylindrical roller bearings equipped with opposing guide flanges.

3. Unique "Double Duty" Applications: (2 of many examples)

    - The bearing race material of a universal joint bearing, per Figures 16 and 17, supports "needle" bearing loads as well as cyclic thrust loads from the end of the trunnion (shaft) creating bending and shear stress at the bottom of the "cup".

    - The washer of an axial ball bearing which functions as a piston driver in a hydraulic pump application per Figure 18, while the race supports the ball bearing load. Bending and shear loads are generated between the balls.

The bearing components noted above, and others not cited, are manufactured as a single part and are uniformly heat treated such that the critical areas in bending or shear are of the same high hardness steel as the race surfaces which see the bearing loads. Using the bearing material for two functions is generally less expensive than having a multiple piece assembly with a varied material selection. With shafting, the concern is not one of considering multiple pieces, but rather from the economics of keeping the entire shaft uniformly heat treated as compared to induction hardening the race area only, to cite one heat treat alternative.

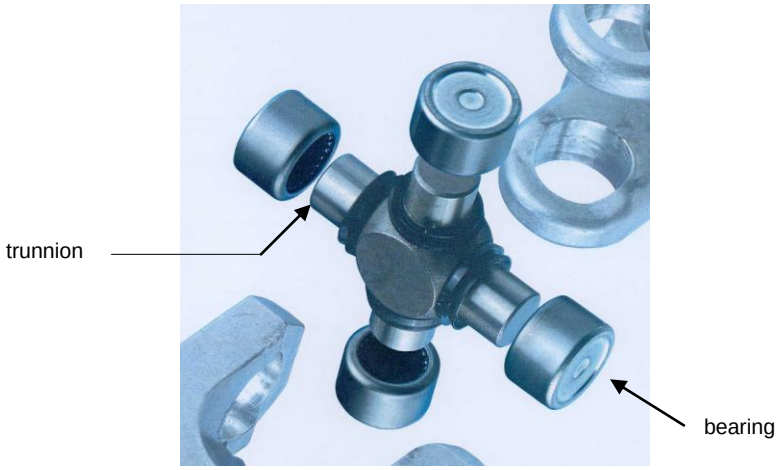

Figure 16. Exploded view of universal joint bearing system with 4 full compliment needle bearings. which see axial force (right) in addition to radial force.

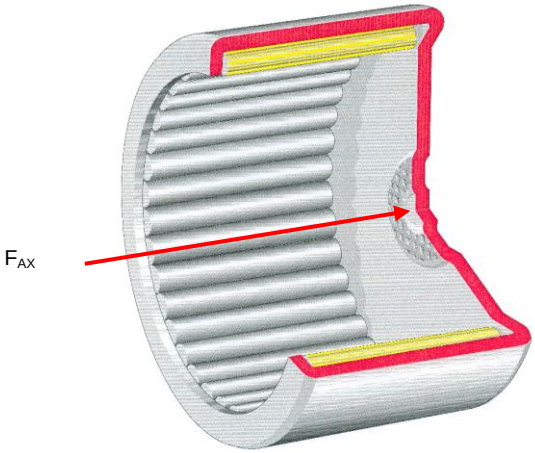

Figure 17. Needle bearings in u-joint see axial force in addition to radial force.

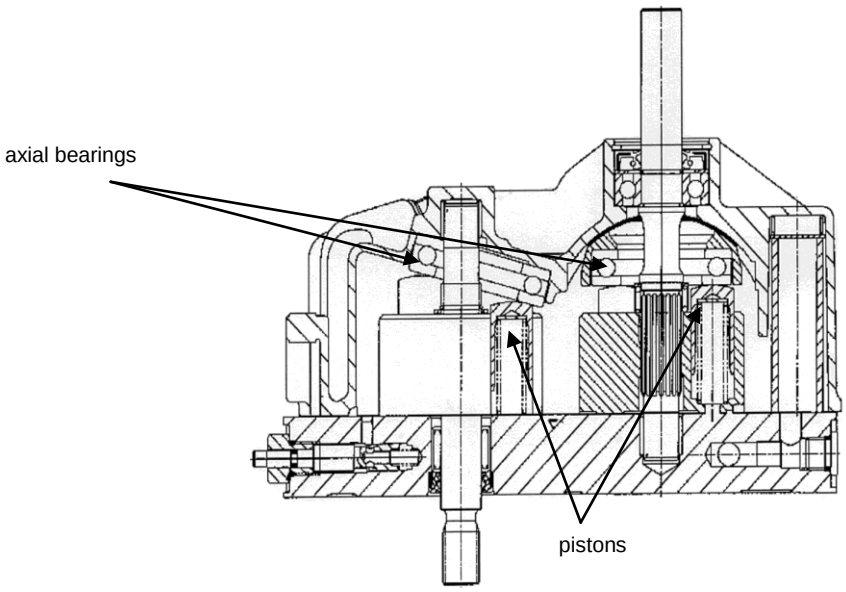

Figure 18. Positive Displacement Pump with axial piston drive with INA ball thrust bearings loaded by hydraulic pistons.

2.5 FATIGUE ASSESSMENT WITH 52100 FINITE LIFE APPLICATIONS

The VPD (Virtual Product Development) capabilities and practices of the worldwide Schaeffler Group are extensive; ranging nearly the entire gamut of today's known CAE tools and more. For infinite life fatigue assessment with stress-life methods, the Schaeffler Group primarily uses standards taken from the FKM guideline (2003). The purpose of this paper, however is to extend some of the VPD experiences related to *finite life* fatigue analysis and testing with bearing grade steel at INA USA. Of particular interest is how the fe-safe™ program has provided correlation with recent fatigue testing and validation at INA USA with SAE52100 bearing steel.

Two applications with SAE52100 bearing races, loaded in a structural manner, were chosen for fatigue analysis to test and compare fe-safe™ finite life cycle results to testing data:

1. INA Tripod Rollers tested in bending and shear as fatigue coupons. (Figure 19)
2. INA Axial Ball Bearings (Figure 18) tested in bending and shear with balls fixed in position.

It should be noted that the testing and analysis made for this purpose represents the SAE52100 capability to endure structural bending loads without rolling contact loads. In the real field applications, the bearing races would typically see rolling contact and bending loads combined. The data and analysis therefore becomes more valuable when considering the SAE52100 for purely structural conditions. Both of these applications were fatigue tested under finite life load

conditions by a simply applied cyclic pulsating ($R \approx 0$) load using standard hydraulically actuated MTS equipment.

2.5.1 Tripod Roller Structural Testing and Analysis:

INA Tripod Rollers as shown in Figure 19 are used in typical CV Joint type automotive applications. Product validation involves several phases; one phase of the validation program is simple fatigue testing of the outer race (roller).

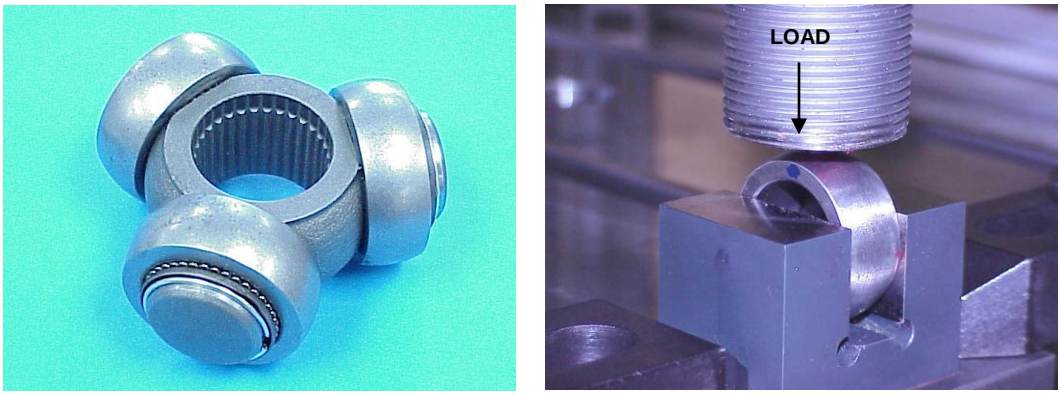

Figure 19. INA USA photos of Tripod Rollers. Assembled in the bearing application prior to CV joint assembly (right) and test setup (left) in MTS station.

The shape and test configuration of the tripod rollers are very convenient for FE analysis and fatigue assessment purposes and make excellent test coupons. With a basic shape and simply applied load, the confidence in the FE stress results are high and the location of the most likely area of concern for fatigue failure is evident. The spherical upper surface of the roller design also serves to guarantee the loading point on the part, even in the case of imperfect test fixture set-up or manufactured geometry, again adding confidence to the analytical results.

For the initial FE analysis of the tripod roller test, static structural FE analysis with ABAQUS/ Standard v6.x was made. In the FEM, the part is loaded on the top of the sphere with a rigid surface and is supported underneath symmetrically (Figure 20) as per the laboratory test set-up. The actual FEM takes advantage of the simple roller geometry and test set-up to section the model with 3 planes of symmetry, creating a "1/8 cut" representation of the real part as shown in Figure 21. The ABAQUS program was easy to setup using surface to surface contact between the elastic body of the tripod roller and rigid surfaces for the tooling. Automatic time increments eased the optimization of the running of the analysis through the load step.

The FE result of interest is the tensile stress along the inner fiber (inner diameter) of the part, directly underneath the applied load. The failure origination of tested real parts was likewise found to be in the area of the inner diameter directly under the load point.

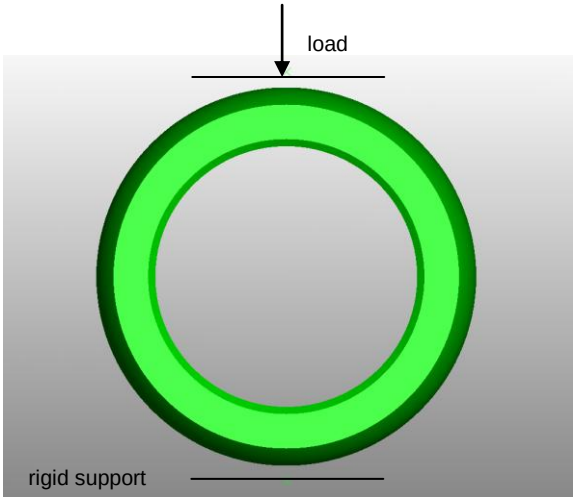

Figure 20. FEM setup of tripod roller fatigue testing with load applied by rigid surface contact on OD.

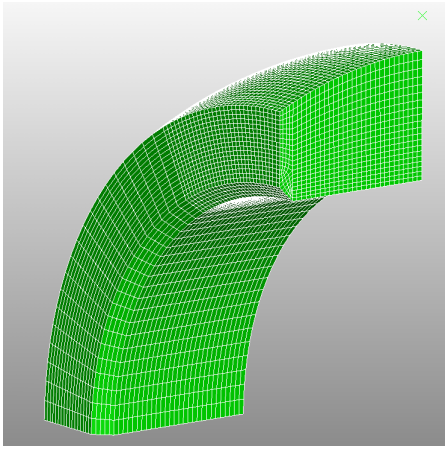

Figure 21. Final meshed FEM of tripod roller with 3 planes of symmetry.

After obtaining static FE stress results, finite life fatigue assessment for the tripod roller was made using fe-safe™ v5.2 from Safe Technology, Ltd. With a simple sinusoidal pulsating load cycle, the inputs for the fe-safe™ program are straightforward using the software GUI.

For this example, the essential fe-safe™ inputs to consider are:

1. FE stress and strain results
2. Proper theory (strain-life, stress-life, Goodman or Morrow correction, etc.)
3. Material properties

4. Load history
5. Surface condition, including residual stress and surface finish (K_T)

For input (1): The FE stress and strain results are read into fe-safe™ as a "dataset" directly from the ABAQUS output file. The main choices to make for the dataset are to select which history steps from the FE model are required, and whether strain results for elastic-plastic analysis are to be read in as well as stresses. For this example, linear elastic stress-strain history is chosen whereby fe-safe™ internally uses Neuber's rule (Draper, 2004) to account for cyclic plasticity in a strain life fatigue analysis.

For input (2): The fatigue theory chosen for the 52100 test and analysis examples is the Brown-Miller strain life criteria with Morrow mean stress correction (Draper 2004). This decision was arrived at after running several fe-safe™ fatigue analyses for the tripod FEA using other available algorithms such as Maximum Principal Strain, Maximum Principal Stress, and Brown-Miller Combined Direct and Shear Stress methods. It was found that the best correlation to real data from fe-safe™ output, including location of expected failures, was made using the Brown-Miller criteria for bi-axial strain life with Morrow mean stress correction (Draper, 2004) per Equation 8.

$$\frac{\gamma}{2}+\frac{\Delta\varepsilon_N}{2}=1.65\frac{\sigma'_f-\sigma_{N,m}}{E}\left(2N_f\right)^b+1.75\varepsilon'_f\left(2N_f\right)^c \tag{8}$$

where:

$\sigma_{N,m}$ = mean normal stress on the (critical) plane,

$2N_f$ = reversals (half - cycle) to crack initiation, $\frac{\gamma}{2}$ = shear strain amplitude,

$\Delta\varepsilon_N$ = normal strain on the critical plane, σ'_f = fatigue strength coefficient,

ε'_f = fatigue ductility coefficient, E = elastic modulus,

c = fatigue ductility (Coffin - Manson) exponent,

b = fatigue strength (Basquins) exponent.

For input (3): The strain life material properties for 52100 were initially taken from the existing default values in the fe-safe™ system database for SAE52100 (Smith, 1963). Some of these values were then modified per approximation methods from the work of Roessle et al. (2000) taking advantage of INA USA SAE52100 test data. It is noted that the INA modifications, while proprietary, did not differ by more than 10% from the fe-safe™ default values.

For input (4): As previously stated, the test loading was a simple cyclic pulsating load with R ≈ 0. The first actual MTS tripod roller test to be analyzed ran with 500 N preload to a 20,000 N maximum load in a sinusoidal pattern. The final history step in the FEA, as selected for the fe-safe™ dataset, represented a total load of 20,000 N. For fe-safe™ to calculate a finite life cycle estimation for this test, a "User Loading" is input as a simple scale factor of the dataset load, which is 20,000 N in this case. Thus for a test with 500 N preload and 20,000 N maximum load,

the scale to the FEA dataset is 0.025 and 1.0, respectively. With this input method, the only necessary change to perform life cycle estimations with higher loads is to increase the scale factor.

For input (5): The inner diameter of the tripod rollers is a bearing race and thus is of bearing quality; that is, the surface finish is very fine, yet not quite mirror polished. The fe-safe™ default method of defining K_T factors, taken from UNI 760, conveniently provides correlation to R_a surface finish measurement values as shown in Figure 22.

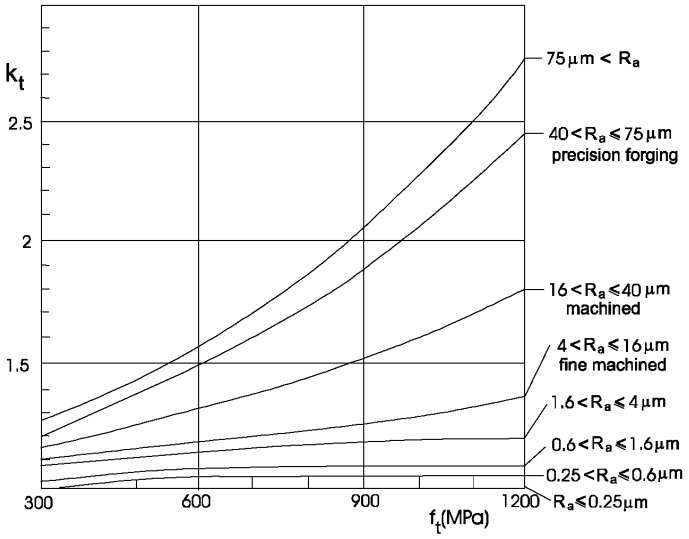

Figure 22. K_T surface finish factor as a function of UTS.

From this method, $K_T = 1.05$ due to surface finish was used for the tripod roller fatigue analysis.

Once the main inputs were chosen, two loading magnitudes were run with fe-safe™ corresponding to two finite life load tests run in the laboratory. The loading details only changed by maximum amplitude for each analysis run, and the results are given in Table 1, below. Note that the fe-safe™ output provides the estimated number of load cycles to fatigue failure *for L_{50} reliability*.

Table 1. Finite Life analysis results from FEA and fe-safe™.

Test	Preload	Upper Load	L_{50} Life per fe-safe™ # cycles
TR20K	500 N	20,000 N	91,600
TR21K	500 N	21,000 N	58,300

The FEA/fatigue assessment results per Table 1 are compared to the laboratory test results from the real tripod rollers, which show good agreement to the analysis of the L_{50} expectations. The two Weibull plots from the testing are provided below in Figures 23 and 24 for real test TR20K and TR21K, respectively. In both cases the fe-safe™ finite life assessment is clearly within the confidence bands of the Weibull data at the L_{50} reliability from real testing.

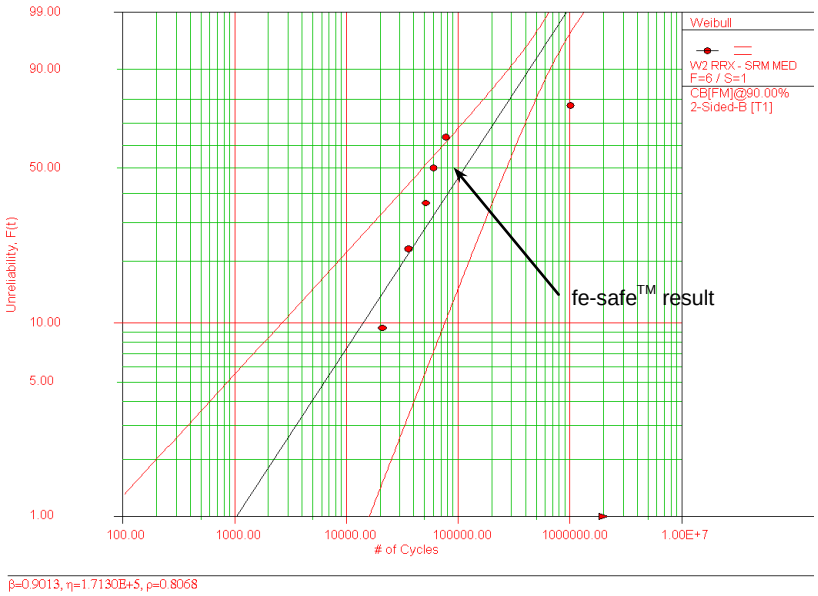

Figure 23. INA USA SAE 52100 fatigue results for tripod roller test TR20K. HRC60-64, Max Load = 20KN, R = 0.025, slope β=0.901, test L_{50} ≈ 110K.

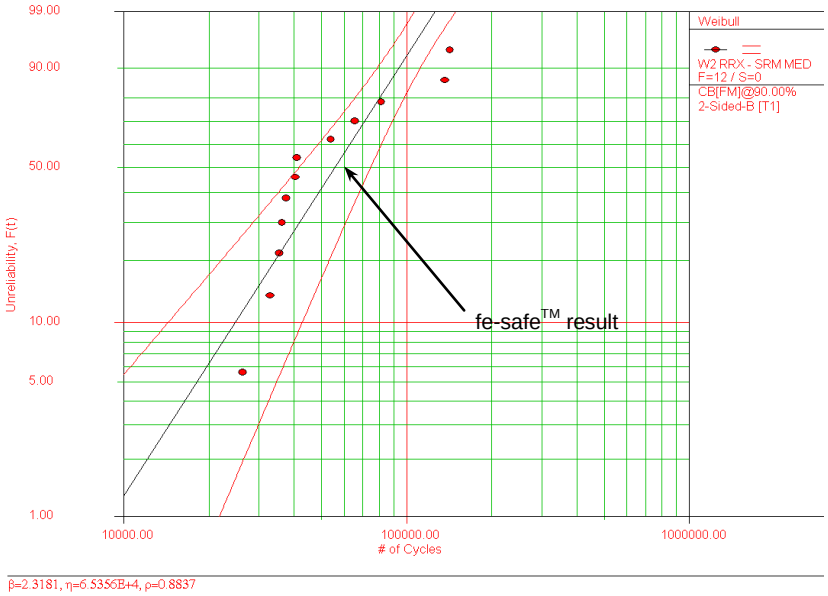

Figure 24. INA USA SAE 52100 fatigue results for tripod roller test TR21K. HRC60-64, Max Load = 21KN, R = 0.0238, slope β=2.318, test L_{50} ≈ 55K.

From the data presented in Figure 23, it is seen that the "as-tested" L_{50} result is about 110K cycles, as compared to the FEA/fe-safe™ assessment of 91.6K cycles. The Weibull slope of 0.9 is again indicative of the wide range expected from bearing grade steel. From the test data it should be noted that out of only 7 tested samples, all made with bearing quality surfaces, the approximate range of results was from 20K cycles up to (a suspension) 2M cycles: 100:1. This extreme range shows the need to test more than 7 parts when higher confidence and reliability from the test results are required.

From the data presented in Figure 24, it can be seen that the "as-tested" L_{50} result for test TR21K is about 55K cycles, as compared to the FEA/fe-safe™ assessment of 58.3K cycles. The Weibull slope of 2.3 shows less scatter in the results as compared to the smaller test load. The range in test results from TR21K was approximately 5.4:1 out of 12 total samples run.

The spread of the confidence bands from Figures 23 and 24 both show that more samples of SAE52100 tripod rollers should be tested to better understand the *range* of fatigue results to be expected in service. However, even from the few samples tested it is clearly observed that very high scatter of fatigue data must be considered when using bearing grade steel in structural applications. From the perspective of validating the Brown-Miller criteria, a very good initial L_{50} finite life fatigue comparison to real data has been made with only minor modification to the default fe-safe™ material and surface recommendations.

2.5.2 Ball Thrust Washer Structural Testing and Analysis:

The next VPD validation study is with an axial ball bearing washer which also functions as a piston driver in a hydraulic pump application per Figure 18 as presented in the previous section. Bending and shear loads are generated between the balls per Figure 25 in laboratory testing and the test results are compared to the FEA/fe-safe™ finite life estimations.

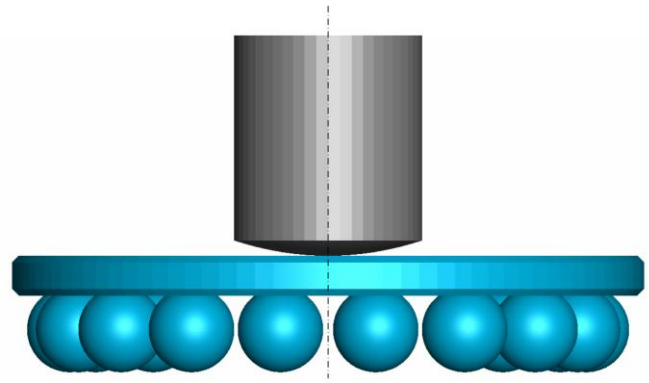

Figure 25. FEM representation of washer loaded by piston between 2 balls.

Finite Element Models were created with ABAQUS/Standard v6.x to simulate the static stresses developed in the washer by the laboratory MTS testing. A single static analysis with one plane of

symmetry is sufficient for the task since the test set-up fixed the balls in position; the testing was therefore structural only, with no cyclic ball loading. Two FEM's were made because the piston location was varied during the real testing as shown in Figures 26 and 27. Both FE models considered elastic body contact between the piston and washer surfaces, and the washer mesh was exactly the same for both.

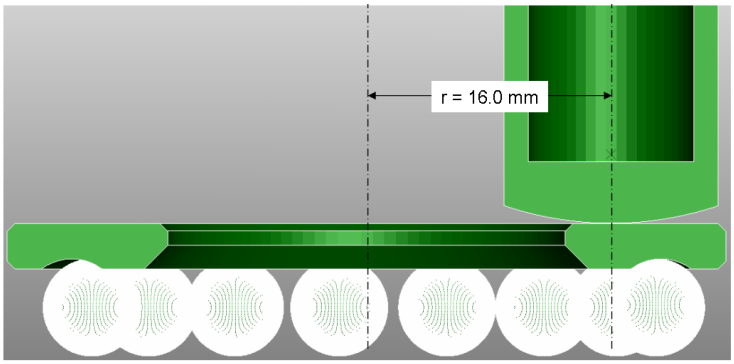

Figure 26. Thrust Washer FEM with piston position at r =16mm from bearing center representing test TW16.0. View shown is 1,2 plane of symmetry.

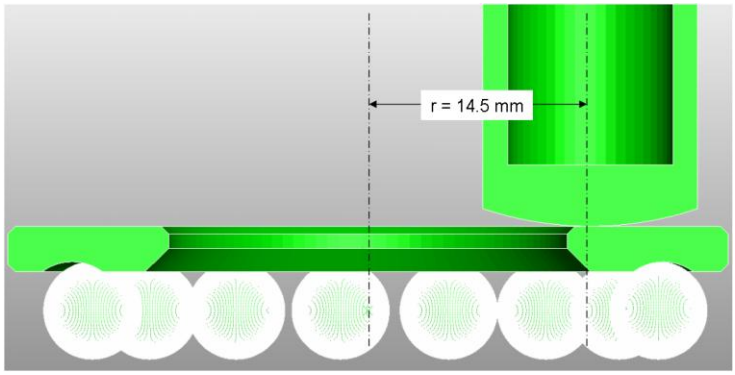

Figure 27. Thrust Washer FEM with piston position at r =14.5mm from bearing center representing test TW14.5. View shown is 1,2 plane of symmetry.

Analysis results from the two FEM's (Figures 26 and 27) show that the worse case tensile stress exists on the inner surface of the washer beneath the loading point of the piston. The FE results from TW14.5 show higher peak tensile stresses (Figure 28) than the TW16.0 model due to the position of the piston. Observed real failures from the laboratory testing verified that the area of fatigue initiation was in the same location as the highest FE tensile stress, and that the TW14.5 test was indeed worse.

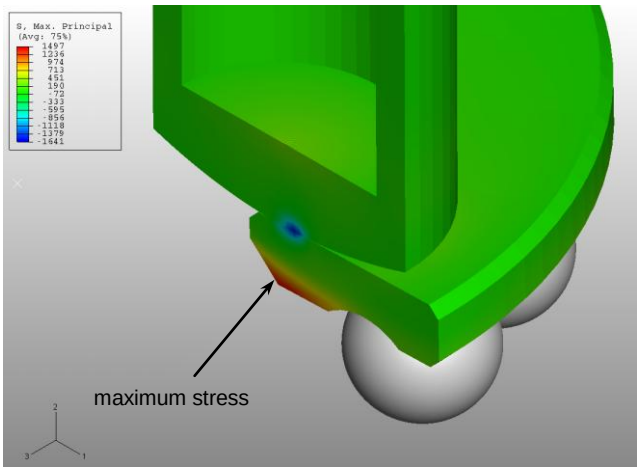

Figure 28. Ball Thrust Washer FE output for maximum prin. stress for FEM TW14.5.

After obtaining the static FE stress results from the thrust washer models, finite life fatigue assessments were made, again using fe-safe™ v5.2. The inputs used for the washer models, including fatigue theory and material properties, were exactly the same as per the tripod rollers. The loading in the real test was again a simple sinusoidal pulsating load cycle, thus only a single history step input of stress for each FEM was required for the dataset, while the load details consisted of a single pulsating load according to the pre and maximum loads per the testing documentation. The only input difference as compared to the tripod roller models is surface finish. The area of interest for the thrust washer is not "bearing quality", but rather it is finely ground. Taking into account the surface finish in the highly stressed area and consulting the chart per Figure 22, which is built into the fe-safe™ defaults as previously discussed, a K_T factor = 1.194 was arrived at for the thrust washer models. The loading, FE stress results, and subsequent fe-safe™ L_{50} life cycle results are given in Table 2, below.

Table 2. FEA and Finite Life analysis Results with fe-safe™. Thrust Washer Analysis TW16.0 and TW14.5.

Test	Preload	Upper Load	FE Tensile Stress	L_{50} Life per fe-safe™ # cycles
TW16.0	130 N	5500 N	1210 MPa	90,700
TW14.5	150 N	5500 N	1650 MPa	6,800

To compare the analysis life cycle output to the real testing, see Figures 29 and 30 which show the Weibull plots from real testing sample groups TW16.0 and TW14.5, respectively.

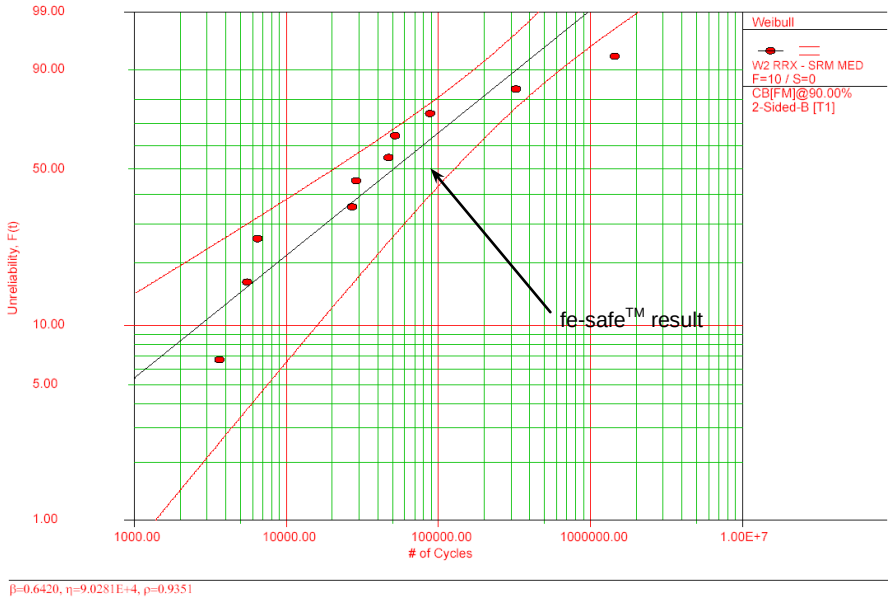

Figure 29. INA USA (2005) SAE 52100 fatigue results for thrust washer test TW16.0. HRC60-64, Max Load = 5500N, R = 0.0236, slope β=0.642, test L_{50} ≈ 50K.

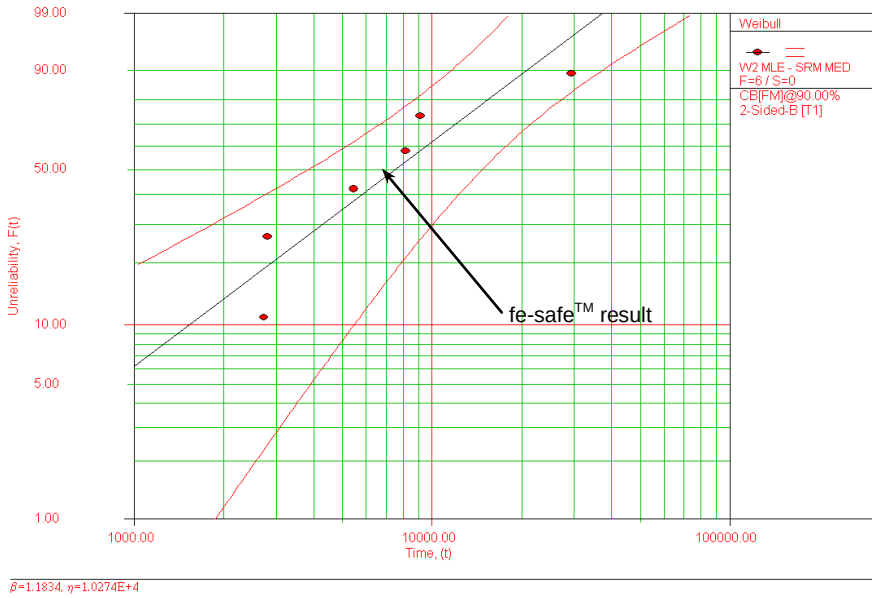

Figure 30. INA USA (2006) SAE 52100 fatigue results for thrust washer test TW14.5. HRC60-64, Max Load = 5500N, R = 0.0272, slope β=1.18, test L_{50} ≈ 7300 cycles.

Upon comparing the finite life analysis results to the real test data, good agreement of the L_{50} assessments are again observed when the Weibull confidence bands are considered. Even though the difference in L_{50} between analysis and real test for TW16.0 was 1.8:1, (90.7K/50K cycles) the fe-safe™ result was still well within the Weibull confidence bands at L_{50}, which extend out to 140K cycles on the high end. The finite life L_{50} ratio between test and analysis for TW14.5 was only 1.1:1 (7500/6800 cycles).

From the high spread of the *confidence bands* on the Weibull plots (Figures 29 and 30) it is apparent that more samples should be tested to gain greater confidence in the L_{50} (or any other reliability) results. The high *range of results* (scatter) as witnessed by the Weibull slopes of 0.64 (Figure 29) and 1.18 (Figure 30) has already been discussed as being the nature of bearing quality SAE52100 when fatigue loaded. The total range of results from test TW16.0 was nearly 400:1 out of 10 samples. The more highly stressed parts from test TW14.5 had a total fatigue cycle range of just over 10:1 with only 6 parts tested. Note again that the total range will also encompass scatter due to minor surface condition differences and minor test set-up error from part to part, yet again clearly shows how intolerant the high hardness steel is to "small" imperfections when fatigued.

Although there is more work to do, as there often is, with the real laboratory testing of these components due to the high confidence band ranges, the L_{50} correlations found so far provide us with good initial validations using FEA with the Brown-Miller fatigue algorithm in fe-safe™.

3. CONCLUSIONS

A brief introduction of the main causes and features of classic material fatigue of rolling bearings was presented along with some of the ramifications of using bearing grade steel in structural fatigue type applications, such as shafts.

Bearing steels will typically realize high scatter in fatigue results, relative to ductile steels, whether used as a bearing or as a structural machine member. Fatigue scatter with bearing steel is due largely to the inconsistent existence of sub-surface non-metallic inclusions randomly located within the volume stressed of the otherwise very strong microstructure. The effect of inclusions follows the fact that *these very high hardness steels are highly notch sensitive, thus it is expected that the fatigue durability of these materials will be greatly diminished by surface imperfections as well as sub-surface inhomogeneities.*

Recent INA USA VPD activities support these conclusions from real testing with bearing grade SAE52100 under finite life fatigue test conditions. It was shown that for these initial finite life VPD validation studies, good fatigue assessment correlations using fe-safe™ were made when considering L_{50} median life. More testing should be made with SAE52100 to increase confidence in the VPD methods used.

4. REFERENCES

1. Harris, T. A., *Rolling Bearing Analysis*, 3rd ed., John Wiley & Sons, 1991.
2. Eschmann, Hasbargen, and Weigand, *Ball and Roller Bearings, Theory, Design, and Application*, 2nd ed., John Wiley and Sons, 1985.

3. Tallian, T. E., *Failure Atlas for Hertz Contact Machine Elements*, 2nd ed., ASME Press, New York, 1999.
4. Hertz, H., "On the Contact of Rigid Elastic Solids and on Hardness," *Miscellaneous Papers*, Macmillan, London, pp. 163-183 (1896).
5. Jones, A. B., *Analysis of Stresses and Deflections*, New Departure Engineering Data, Bristol, CT, pp. 12-22, 1946.
6. Shigley, J. E., and Mischke, C. R., *Mechanical Engineering Design*, 5th ed., Mc-Graw-Hill, 1989.
7. Dieter, G., *Mechanical Metallurgy*, 3rd ed., Mc-Graw-Hill, 1986.
8. International Standard ISO 281, 1st ed., 1990-12-01, *Rolling Bearings – Dynamic Load Ratings and Rating Life*, 1990.
9. Lundberg, G., and Palmgren, A., "Dynamic Capacity of Rolling Bearings," *Acta Polytech*. Mechanical Engineering Series, Royal Swedish Academy of Engineering Sciences, Vol. 1 Nos. 3, 7, 1947.
10. Weibull, W., "A Statistical Theory of the Strength of Materials," *Proc. R. Swedish Inst. Eng. Res.*, No,. 151, Stockholm, 1939.
11. Murthy, D. N., Xie, M., and Jiang, R., *Weibull Models*, Wiley-I.E.E.E., 2003.
12. ASM Handbook, Vol. 11, *Failure Analysis and Prevention*, ASM International, Metals Park, OH., 2002, pp. 627 – 648.
13. Schlicht, H., Schreiber, E., and Zwirlein, O., "Effects of Material Properties on Bearing Steel Fatigue Strength", *Effect of Steel Manufacturing Processes on the Quality of Bearing Steels, ASTM STP 987*, J.J.C. Hoo, Ed., ASTM, Philadelphia, 1988, pp. 81-101.
14. Voskamp, A. P., and Hollox, G. E., "Failsafe Rating of Ball Bearing Components," *Effect of Steel Manufacturing Processes on the Quality of Bearing Steels, ASTM STP 987*, J.J.C. Hoo, Ed., ASTM, Philadelphia, 1988, pp. 102-112.
15. Pearson, P. K., and Dickenson, T. W., "The Role of Carbides in Performance of High-Alloy Bearing Steels," *Effect of Steel Manufacturing Processes on the Quality of Bearing Steels, ASTM STP 987*, J.J.C. Hoo, Ed., ASTM, Philadelphia, 1988, pp. 113-131.
16. Richard S. Carpenter, Corporate Metallurgist, Schaeffler Group USA, Inc., discussion notes, 16 Aug. 2006.
17. ASTM, Std. A295-98, "High Carbon Ball and Rolling Bearing Steels;" Std. A485-94, "High Hardenability Bearing Steels," ASTM, Philadelphia.
18. ASTM, Std. E112-96, "Standard Test Methods for Determining Average Grain Size," ASTM, Philadelphia.
19. Hertzberg, R. W., "*Deformation and Fracture Mechanics of Engineering Materials*," 4th ed., John Wiley & Sons, 1996.
20. Zwirlein, O., Mützel, R., and Schlicht H., "Prüfung Gehärteter Stähle im Zugversuch," (HTM 31 (1976) 5, S. 277-286).
21. Stangner, H., "Werkstoffe für Wälzlager – Festigkeitsverhalten, Auswahlkriterien" (VDI-Berichte 600.1 (1986), S. 421-438).

22. Green, W. B., "A Brief History, Status, and Mission of ASTM subcommittee A01.28 on Bearing Steels," *Bearing Steels: Into the 21st Century, ASTM STP 1327*, J.J.C. Hoo and W. B. Green, Eds., American Society for Testing and Materials, 1998, pp 3-9.

23. Hampshire, J. M., and King, E., "Quantitative Inclusion Ratings and Continuous Casting: User Experience and Relationships with Rolling Contact Fatigue Life," *Effect of Steel Manufacturing Processes on the Quality of Bearing Steels, ASTM STP 987*, J.J.C. Hoo, Ed., ASTM, Philadelphia, 1988, pp. 61-80.

24. Monnot, J., Heritier, B., and Cogne, J., "Relationship of Melting Practice, Inclusion Type, and Size with Fatigue Resistance of Bearing Steels," *Effect of Steel Manufacturing Processes on the Quality of Bearing Steels, ASTM STP 987*, J.J.C. Hoo, Ed., ASTM, Philadelphia, 1988, pp. 149-165.

25. Zaretsky, E. V., "Selection of Rolling-Bearing Steels for Long-Life Applications," *Effect of Steel Manufacturing Processes on the Quality of Bearing Steels, ASTM STP 987*, J.J.C. Hoo, Ed., ASTM, Philadelphia, 1988, pp. 5-43.

26. Lormand, G., Meynaud, P., Vincent, A., Baudry, G., Girodin, D., and Dudragne, G., "From Cleanliness to Rolling Fatigue Life of Bearings – A New Approach" *Bearing Steels: Into the 21st Century, ASTM STP 1327*, J.J.C. Hoo and W. B. Green, Eds., ASTM, 1998, pp. 55-69.

27. Weibull, W., "Fatigue Testing and the Analysis of Results," Journal of Applied Mechanics, Vol 18, no. 3, pp.293-297, 1951.

28. Stephens, R. I., Fatemi, A., Stephens, R. R., and Fuchs, H. O., *Metal Fatigue in Engineering*, 2nd ed., John Wiley & Sons, 2001.

29. Socie, D. F., and Marquis, G. B., *Multiaxial Fatigue*, Society of Automotive Engineers, Inc., Warrendale, PA, 2000.

30. Juvinall, R. C., and Marshek, K. M., *Fundamentals of Machine Component Design*, 2nd ed., John Wiley & Sons, 1991.

31. Laird, C., "Mechanisms and Theories of Fatigue," *Fatigue and Microstructure*," American Society for Metals, Metals Park, Ohio, 1979, pp. 148-203.

32. Laird, C., "Fatigue Crack Propagation," ASTM Spec. Tech Publ. 415, pp. 131-168, 1967.

33. Forrest, P. G., *Fatigue of Metals*, Pergamon Press, Ltd., 1962.

34. FKM-Guideline, Analytical Strength Assessment of Components in Mechanical Engineering, 5th ed., English Version Translation by E. Haibach, VDMA Verlag GmbH, Frankfurt a.M., 2003. ISBN 3-8163-0425-7

35. Draper, J., Modern Metal Fatigue Analysis, Course Notes, Safe Technology Limited, Sheffield, UK, 2004.

36. Smith, R. W., Hirschberg, M. H., and Manson, S. S., Fatigue Behavior of Metals in Low and Intermediate Life Ranges, NASA Technical Note D-1574, 1963.

37. Roessle, M. L., and Fatemi, A., Strain-controlled fatigue properties of steels and some simple approximations, *International Journal of Fatigue*, 22, 2000, pp 495-511.

38. UNI 760, *Meccanismi per Apparecchi di Sollevamento*, UNI-Ente Nazionale Italiano Di Unificazione, 20133 Milano, via Battistotti Sassi, 11b, Italy.

5. ACKNOWLEDEMENTS

Richard S. Carpenter, Corporate Metallurgist, Schaeffler Group USA, Inc.
Bearing fatigue and steel metallurgy

Anthony P. Reynolds, PhD., Associate Professor, University of South Carolina
Fatigue crack growth analysis